

# Solid-state $^{25}\text{Mg}$ NMR, X-ray crystallographic, and quantum mechanical study of bis(pyridine)-(5,10,15,20-tetraphenylporphyrinato)magnesium(II)

Gang Wu, Alan Wong, and Suning Wang

**Abstract:** We report solid-state  $^{25}\text{Mg}$  NMR, X-ray crystallographic, and quantum-mechanical calculation results for bis(pyridine)(5,10,15,20-tetraphenylporphyrinato)magnesium(II),  $\text{Mg}(\text{TPP})\cdot\text{Py}_2$ .  $\text{Mg}(\text{TPP})\cdot\text{Py}_2$  crystallizes in the triclinic form, in the space group  $P\bar{1}$ . The unit cell parameters are:  $a = 9.6139(13)$  Å,  $b = 11.0096(16)$  Å,  $c = 11.8656(15)$  Å;  $\alpha = 102.063(3)^\circ$ ,  $\beta = 103.785(3)^\circ$ ,  $\gamma = 114.043(2)^\circ$ ;  $Z = 1$ . The Mg(II) ion is coordinated to four nitrogen atoms from the porphyrin ring and two nitrogen atoms from the axial pyridine ligands, forming a regular octahedron. The  $^{25}\text{Mg}$  quadrupole coupling constant ( $C_Q$ ) is  $15.32 \pm 0.02$  MHz, which represents the largest value so far observed for  $^{25}\text{Mg}$  nuclei. The electric field gradient tensor at the Mg site is axially symmetric,  $\eta_Q = 0.00 \pm 0.05$ . The  $^{25}\text{Mg}$  chemical shielding anisotropy is too small to be accurately determined. Quantum-mechanical calculations using a 6–31G(d) basis set reproduce reasonably well the observed  $^{25}\text{Mg}$  NMR data for  $\text{Mg}(\text{TPP})\cdot\text{Py}_2$ . The calculations also suggest that the span of the  $^{25}\text{Mg}$  chemical shift tensor is less than 50 ppm. Using a theoretical approach, we also investigate the dependence of the  $^{25}\text{Mg}$  quadrupole coupling constant on the  $\text{Mg}-\text{N}_{\text{ax}}$  bond distance. The calculation suggests that the  $^{25}\text{Mg}$  quadrupole coupling constant for an Mg(II) ion at the center of a porphyrin ring without axial ligands is approximately 22 MHz, which may be treated as an upper limit of the  $^{25}\text{Mg}$  quadrupole coupling constant for all Mg–porphyrin complexes.

**Key words:**  $^{25}\text{Mg}$  NMR, crystal structure, quantum chemical calculation, quadrupole parameter, tetraphenylporphyrin.

**Résumé :** Dans ce travail, on rapporte les résultats d'études RMN du  $^{25}\text{Mg}$ , de diffraction des rayons X et de calculs théoriques de mécanique quantique sur la bis(pyridine)(5,10,15,20-tétraphénylporphyrinato)magnésium(II),  $\text{Mg}(\text{TPP})\cdot\text{Py}_2$ . Le  $\text{Mg}(\text{TPP})\cdot\text{Py}_2$  cristallise dans la forme triclinique, groupe d'espace  $P\bar{1}$ , avec  $a = 9,6139(13)$  Å,  $b = 11,0096(16)$  Å et  $c = 11,8656(15)$  Å;  $\alpha = 102,063(3)^\circ$ ,  $\beta = 103,785(3)^\circ$  et  $\gamma = 114,043(2)^\circ$  et  $Z = 1$ . L'ion Mg(II) est coordonné à quatre atomes d'azote du noyau porphyrine et à deux atomes d'azote des ligands pyridine axiaux et il forme un octaèdre régulier. La constante de couplage quadripolaire du  $^{25}\text{Mg}$  ( $C_Q$ ) est de  $15,32 \pm 0,02$  MHz, ce qui correspond à la valeur la plus élevée jusqu'à maintenant pour le noyau  $^{25}\text{Mg}$ . Le tenseur du gradient du champ électrique au niveau du site Mg présente une symétrie axiale avec  $\eta_Q = 0,00 \pm 0,05$ . L'anisotropie de blindage chimique du  $^{25}\text{Mg}$  est trop faible pour être mesurée de façon fiable. Des calculs de mécanique quantique effectués à l'aide d'un ensemble de base 6-31G(d) permettent de reproduire raisonnablement les données observées par RMN du  $^{25}\text{Mg}$  pour le  $\text{Mg}(\text{TPP})\cdot\text{Py}_2$ . Les calculs suggèrent aussi que la plage du tenseur du déplacement chimique du  $^{25}\text{Mg}$  est inférieure à 50 ppm. Faisant appel à une approche théorique, on a aussi étudié la dépendance de la constante de couplage quadripolaire du  $^{25}\text{Mg}$  sur la longueur de la liaison  $\text{Mg}-\text{N}_{\text{ax}}$ . Les calculs suggèrent que la constante de couplage quadripolaire du  $^{25}\text{Mg}$  pour l'ion Mg(II) au centre d'un noyau porphyrine sans ligands axiaux est d'environ 22 MHz, ce qui peut être considéré comme une limite supérieure pour la constante de couplage quadripolaire du  $^{25}\text{Mg}$  pour tous les complexes Mg–porphyrine.

**Mots clés :** RMN du  $^{25}\text{Mg}$ , structure cristalline, calculs de mécanique quantique chimique, paramètre quadripolaire, tétraphénylporphyrine.

[Traduit par la Rédaction]

## Introduction

Metalloporphyrins have been extensively studied for many years because of their biological and catalytic functions (1–3). Several spectroscopic techniques such as EPR (4), NMR (5), and Mössbauer spectroscopy (6) have been used to di-

rectly probe the metal centers in metalloporphyrin systems. Magnesium porphyrins represent an important class of metalloporphyrin compounds because of their relevance to chlorophyll (7). Until now it has not been possible to directly study the Mg(II) ion in Mg–porphyrin complexes by  $^{25}\text{Mg}$  (spin:  $-5/2$ ) NMR. The  $^{25}\text{Mg}$  nucleus is among a group

Received 7 January 2003. Published on the NRC Research Press Web site at <http://canjchem.nrc.ca> on 9 April 2003.

Gang Wu,<sup>1</sup> Alan Wong, and Suning Wang. Department of Chemistry, Queen's University, Kingston, ON K7L 3N6, Canada.

<sup>1</sup>Corresponding author (e-mail: [gangwu@chem.queensu.ca](mailto:gangwu@chem.queensu.ca)).

of low- $\gamma$  quadrupolar nuclides that are known to be notoriously difficult to study by NMR. Although solution  $^{25}\text{Mg}$  NMR techniques have been applied to many chemical and biological systems, including proteins and nucleic acids (8), the scope of applications is severely restricted to cases where either the cation exchange is fast or the  $\text{Mg}(\text{II})$  ion is at a symmetrical site, avoiding the unfavorable consequence of rapid  $^{25}\text{Mg}$  quadrupolar relaxation. When an  $\text{Mg}(\text{II})$  ion is tightly bound to a biological macromolecule, the molecular rotational correlation time of the complex is determined by the macromolecule and may be on the order of tens of nanoseconds. Under such a circumstance, the quadrupolar relaxation is so efficient that  $^{25}\text{Mg}$  NMR signals may become too broad to be detected.

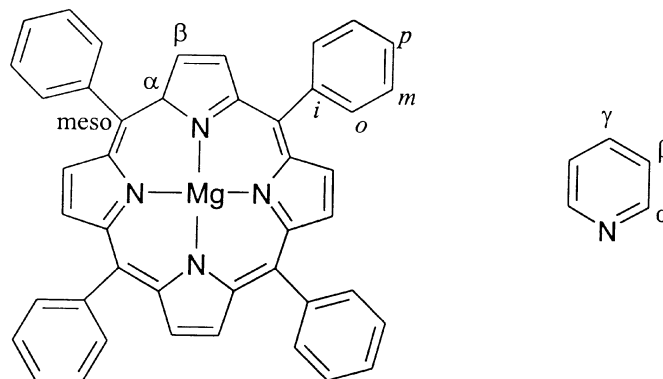
With recent advances in NMR methodology and high-field magnet technology, solid-state NMR has been recognized as a viable technique for studying half-integer quadrupolar nuclei. Previous solid-state  $^{25}\text{Mg}$  NMR studies have almost exclusively focused on inorganic systems (9). In addition, all reported  $^{25}\text{Mg}$  nuclear quadrupole coupling constants are relatively small (ca.  $<9$  MHz). Recently, two research groups have extended solid-state  $^{25}\text{Mg}$  NMR to organic systems. More specifically, Sham and Wu reported a solid-state  $^{25}\text{Mg}$  NMR study of several  $\text{Mg}(\text{II})$  coordination complexes (10). These compounds were used as models for inner-sphere Mg binding often found in nucleic acids. Frydman and co-workers obtained solid-state  $^{25}\text{Mg}$  NMR spectra for an  $\text{Mg}(\text{II})$  adenosine 5'-triphosphate (ATP) complex (11). These two studies demonstrate the great potential of solid-state  $^{25}\text{Mg}$  NMR in probing the  $\text{Mg}(\text{II})$  binding environment in biomolecular systems. In this paper we report the first set of solid-state  $^{25}\text{Mg}$  NMR data for an  $\text{Mg}(\text{II})$ -porphyrin system. To make the solid-state  $^{25}\text{Mg}$  NMR experiment feasible, we prepared  $^{25}\text{Mg}$  isotopically enriched bis(pyridine)(5,10,15,20-tetraphenylporphyrinato)magnesium(II),  $^{25}\text{Mg}(\text{TPP})\cdot\text{Py}_2$ . We also determined the molecular and crystal structures of  $\text{Mg}(\text{TPP})\cdot\text{Py}_2$  by single crystal X-ray crystallography. To better understand the  $^{25}\text{Mg}$  NMR properties and to examine their relationship to molecular structure, we carried out extensive quantum mechanical calculations for the electric field gradient and chemical shielding tensors in two  $\text{Mg}$ -porphyrin systems.

## Experimental details

### Sample preparation

Labeled  $^{25}\text{Mg}(\text{ClO}_4)_2$  (272 mg) was prepared by dissolving 50 mg of  $^{25}\text{MgO}$  ( $^{25}\text{Mg}$  99.1%, purchased from Trace Science International, Toronto, Canada) in  $\text{HClO}_4(\text{aq})$  and evaporating to dryness. The labeled  $^{25}\text{Mg}(\text{TPP})\cdot\text{Py}_2$  complex was prepared following the method described in the literature (12, 13). To a pyridine solution containing 310 mg of 5,10,15,20-tetraphenyl-21*H*, 23*H*-porphine (99+% obtained from Aldrich Chemicals Co., Canada) was added 225 mg of  $^{25}\text{Mg}(\text{ClO}_4)_2$ . The solution was gently refluxed for 12 h in

Scheme 1.



darkness and then evaporated to dryness in a rotary evaporator. The resulting purple precipitate was then washed three times with cold distilled water.  $^1\text{H}$  NMR (400.13 MHz,  $\text{CDCl}_3$ , 298 K) (ppm)  $\delta$ : 8.92 (s, 8H, pyrrole), 8.26 (d, 8H, *o*-phenyl), 7.75 (m, 12H, *m,p*-phenyl), 7.07 (t, 2H,  $\gamma$ -pyridine), 6.49 (t, 4H,  $\beta$ -pyridine), 5.92 (d, 4H,  $\alpha$ -pyridine).  $^{13}\text{C}$  NMR (100.61 MHz,  $\text{CDCl}_3$ , 298 K) (ppm)  $\delta$ : 150.25 (q,  $\alpha$ -pyrrole), 146.93 (t,  $\alpha$ -pyridine), 143.84 (q, *i*-phenyl), 135.87 (t,  $\gamma$ -pyridine), 134.68 (t, *o*-phenyl), 131.80 (t,  $\beta$ -pyrrole), 126.20 (t, *m*-phenyl), 127.03 (t, *p*-phenyl), 122.96 (t,  $\beta$ -pyridine), 121.65 (q, meso). The atomic labeling scheme is shown in Scheme 1.

### Solid-state NMR

Solid-state  $^{25}\text{Mg}$  NMR spectra were recorded on a Bruker Avance-500 (11.75 T) digital NMR spectrometer operating at 30.6 MHz for  $^{25}\text{Mg}$  nuclei. The radio frequency (RF) field strength at the  $^{25}\text{Mg}$  frequency was approximately 50 kHz. A single-channel wideline probe (5 mm insert) was used. A Hahn echo sequence (14) was employed to acquire static  $^{25}\text{Mg}$  NMR spectra:  $P_1(\phi_1) - \tau_1 - P_2(\phi_2) - \tau_2 - \text{Acq}(\phi_3)$ , where  $\phi_1 = x, x, x, x, y, y, y, y, -x, -x, -x, -x, -y, -y, -y, -y$ ;  $\phi_2 = 4 \times (x, y, -x, -y)$ ;  $\phi_3 = -y, y, -y, y, -x, x, -x, x, y, -y, y, -y, x, -x, x, -x$ . The radio-frequency (RF) pulse widths were  $P_1 = 1.50 \mu\text{s}$  and  $P_2 = 3.20 \mu\text{s}$ . The delay between the two RF pulses,  $\tau_1$ , was 400  $\mu\text{s}$ . A much shorter delay was chosen between  $P_2$  and acquisition ( $\tau_2 = 30 \mu\text{s}$ ) so that a whole echo signal could be obtained. Recycle delays of 1 and 2 s were used. To record the very short-lived free induction decay (FID) signals, a 12-bit fast digitizer was used with a dwell time of 0.5  $\mu\text{s}$ , corresponding to a spectral window of 1 MHz. A sample of  $\text{MgO}(\text{s})$  was used as a secondary chemical-shift reference,  $\delta = 26$  ppm (15).

### X-ray crystallography

Crystallographic data for  $\text{Mg}(\text{TPP})\cdot\text{Py}_2$  were collected from a shiny red-purple, hexagonal-shaped crystal (0.1 mm  $\times$  0.2 mm  $\times$  0.4 mm) obtained by slow recrystallization from pyridine.<sup>2</sup> The X-ray diffraction data were col-

<sup>2</sup>Two tables containing hydrogen atom coordinates and anisotropic displacement parameters for  $\text{Mg}(\text{TPP})\cdot\text{Py}_2$  have been deposited as supplementary data. Supplementary data may be purchased from the Depository of Unpublished Data, Document Delivery, CISTI, National Research Council Canada, Ottawa, ON K1A 0S2, Canada ([http://www.nrc.ca/cisti/irm/unpub\\_e.shtml](http://www.nrc.ca/cisti/irm/unpub_e.shtml) for information on ordering electronically). CCDC 205592 contain the supplementary data for this paper. These data can be obtained, free of charge, via [www.ccdc.cam.ac.uk/conts/retrieving.html](http://www.ccdc.cam.ac.uk/conts/retrieving.html) (or from the Cambridge Crystallographic Data Centre, 12 Union Road, Cambridge, U.K.; fax +44 1223 336033; or [deposit@ccdc.cam.ac.uk](mailto:deposit@ccdc.cam.ac.uk)).

lected on a Siemens P4 single-crystal diffractometer with graphite-monochromated Mo  $K\alpha$  radiation, operating at 50 kV and 40 mA at 296 K. Data were corrected for Lorentz and polarization effects and analyzed using the Siemens SHELXTL software package (16). The structure was solved by direct methods. Neutral atom scattering factors were taken from Cromer and Waber (17).

### Quantum mechanical calculations

All quantum mechanical calculations were performed on a SunFire 6800 symmetric multiprocessor system (24 × 900 MHz processors and 24 GB of memory) using the Gaussian98 suite of programs (18). For each calculation, 4 or 8 processors were allocated. For  $^{25}\text{Mg}$  EFG calculations, the following convention was used for the nuclear quadrupole coupling constant ( $C_Q$ ) and the asymmetry parameter ( $\eta_Q$ ):

$$[1] \quad C_Q[\text{MHz}] = \frac{eQV_{ZZ}}{h} = -46.85 \times V_{ZZ} [\text{au}]$$

$$[2] \quad \eta_Q = \frac{V_{XX} - V_{YY}}{V_{ZZ}}$$

where  $V_{ZZ}$ ,  $V_{YY}$ , and  $V_{XX}$  are the principal components of the EFG tensor ( $|V_{ZZ}| \geq |V_{YY}| \geq |V_{XX}|$  and  $V_{ZZ} + V_{YY} + V_{XX} = 0$ ). The coefficient in eq. [1] is obtained using the  $^{25}\text{Mg}$  quadrupole moment value recommended by Pyykkö,  $Q(^{25}\text{Mg}) = 19.94 \times 10^{-30} \text{ m}^2$  (19). The computed EFG tensor components are reported in atomic units (1 au =  $9.717365 \times 10^{21} \text{ V m}^{-2}$ ).

To calculate  $^{25}\text{Mg}$  magnetic shielding tensors, the Gauge including atomic orbital (GIAO) method (20), as implemented in Gaussian98, was used. Because GIAO magnetic shielding calculations are in general more time consuming than EFG calculations, we employed a simplified molecular model to reduce computational time. In particular, the four phenyl groups in TPP were replaced by hydrogen atoms, resulting in a 59-atom model, which is significantly smaller than the total number of atoms in  $\text{Mg}(\text{TPP})\cdot\text{Py}_2$ , 99. To confirm the validity of the 59-atom model, we performed several tests in which calculations were done for both the complete molecule and the simplified model. The shielding tensor results are essentially the same for both clusters, while the computational cost for the 59-atom model was significantly smaller than that for the 99-atom cluster. For example, the HF/6-311G(2d,p) calculation gave  $\sigma_{11} = 571$ ,  $\sigma_{22} = 578$ , and  $\sigma_{33} = 616$  ppm for the 59-atom model with a CPU time of 23 h. In comparison, the CPU time for the complete 99-atom molecule at the same level of theory was 84 h and the  $^{25}\text{Mg}$  magnetic shielding tensor components were:  $\sigma_{11} = 571$ ,  $\sigma_{22} = 578$ , and  $\sigma_{33} = 613$  ppm. Therefore, we have assumed that the 59-atom model can be safely used for all shielding calculations.

## Results and discussion

### Crystal structure

$\text{Mg}(\text{TPP})\cdot\text{Py}_2$  crystallizes in triclinic form (space group,  $P\bar{1}$ ). The Mg(II) ion is located at the origin (0, 0, 0), which is also the center of inversion. The Mg(II) ion, lying in the approximate porphyrin plane, is coordinated to six nitrogen

**Table 1.** Crystallographic data and structure refinement for  $\text{Mg}(\text{TPP})\cdot\text{Py}_2$ .

Empirical formula	$\text{C}_{54} \text{H}_{38} \text{N}_6 \text{Mg}$
Formula weight	795.22
Temperature (K)	293(2)
Wavelength (Å)	0.71073
Crystal system	Triclinic
Space group	$P\bar{1}$
Unit cell dimensions	$a = 9.6139(13) \text{ Å}$ $b = 11.0096(16) \text{ Å}$ $c = 11.8656(15) \text{ Å}$ $\alpha = 102.063(3)^\circ$ $\beta = 103.785(3)^\circ$ $\gamma = 114.043(2)^\circ$
Volume (Å <sup>3</sup> )	1045.5(2)
Z	1
Density (calculated) (g cm <sup>-3</sup> )	1.263
Absorption coefficient (mm <sup>-1</sup> )	0.089
Max. and min. transmission	1.000 and 0.663
Crystal size (mm <sup>3</sup> )	0.1 × 0.2 × 0.4
θ range for data collection (°)	1.88–23.31
Index ranges	$-10 \leq h \leq 10$ , $-12 \leq k \leq 12$ , $-13 \leq l \leq 9$
Reflections collected	5436
Independent reflections	3019 ( $R_{\text{int}} = 0.0350$ )
Completeness to $\theta = 23.31^\circ$ (%)	99.7
Refinement method	Full-matrix least-squares on $F^2$
Data/restraints/parameters	3019/0/293
Goodness-of-fit on $F^2$	0.807
Final $R$ indices [ $I > 2\sigma(I)$ ]	$R_1 = 0.0426$ , $wR_2 = 0.0819$
$R$ indices (all data)	$R_1 = 0.0872$ , $wR_2 = 0.0911$

atoms in a distorted octahedral fashion. Detailed crystallographic data, atomic coordinates, and selected structural parameters are reported in Tables 1, 2, and 3, respectively. As shown in Fig. 1, the four equatorial nitrogen atoms are from the porphyrin moiety and the two remaining axial nitrogen ligands are pyridine molecules. The most important structural feature in  $\text{Mg}(\text{TPP})\cdot\text{Py}_2$  is that the Mg— $\text{N}_{\text{eq}}$  bond lengths, 2.062 and 2.065 Å, are significantly shorter than that for the Mg— $\text{N}_{\text{ax}}$  bond, 2.369 Å. Several precedents exist in the literature for long Mg— $\text{N}_{\text{ax}}$  bonds in Mg-porphyrin systems. For example, the Mg— $\text{N}_{\text{ax}}$  bond length in  $\text{Mg}(\text{TPP})\cdot(\text{piperdine})_2$  is 2.419 Å (21). For  $\text{Mg}(\text{octaethylporphyrin})\cdot\text{Py}_2$  and  $\text{Mg}(\text{TPP})\cdot(4\text{-picoline})_2$ , the Mg— $\text{N}_{\text{ax}}$  bonds are 2.389 and 2.386 Å, respectively (21, 22), which are both very similar to that in  $\text{Mg}(\text{TPP})\cdot\text{Py}_2$ . In contrast, the Mg— $\text{N}_{\text{ax}}$  distance for  $\text{Mg}(\text{TPP})\cdot(1\text{-methylimidazole})_2$  is much shorter, 2.297 Å (21). Because in all these systems the Mg(II) ion is at the center of the porphyrin ring, not surprisingly, the Mg— $\text{N}_{\text{eq}}$  bond distances are essentially the same. The porphyrin core is slightly non-planar. The dihedral angle between the mean pyridine plane and the mean porphyrin plane is 70°. As seen from Fig. 1, the four phenyl groups exhibit two unique orientations with respect to the mean plane of the porphyrin core, 60 and 80°. Clearly, the two different orientations of the phenyl groups are related to the orientation of the pyridine ring. Other structural features regarding the TPP moiety are expected from previous exam-

**Table 2.** Atomic coordinates ( $\times 10^4$ ) and equivalent isotropic displacement parameters ( $\text{\AA}^2 \times 10^3$ ) for  $\text{Mg}(\text{TPP})\text{Py}_2$ .

	<i>x</i>	<i>y</i>	<i>z</i>	U(eq)
Mg(1)	0	0	0	47(1)
N(1)	436(3)	2304(2)	965(2)	54(1)
C(1)	-677(4)	2706(4)	608(3)	66(1)
N(2)	1040(2)	-180(2)	1647(2)	43(1)
C(2)	-424(4)	4065(4)	1006(3)	75(1)
N(3)	2296(2)	1007(2)	-82(2)	43(1)
C(3)	1072(5)	5096(4)	1827(3)	85(1)
C(4)	2245(4)	4720(4)	2214(3)	100(1)
C(5)	1870(4)	3336(4)	1769(3)	81(1)
C(6)	-2176(3)	-2404(3)	2728(2)	46(1)
C(7)	-2845(3)	-3851(3)	2371(3)	65(1)
C(8)	-3403(4)	-4572(3)	3125(3)	75(1)
C(9)	-3307(3)	-3861(4)	4245(3)	64(1)
C(10)	-2677(4)	-2437(4)	4613(3)	70(1)
C(11)	-2120(3)	-1712(3)	3852(3)	62(1)
C(12)	5632(3)	1499(3)	2713(2)	44(1)
C(13)	6186(3)	2428(3)	3908(2)	58(1)
C(14)	7800(4)	3042(3)	4685(3)	70(1)
C(15)	8850(4)	2696(4)	4278(3)	70(1)
C(16)	8323(3)	1745(3)	3135(3)	67(1)
C(17)	6721(3)	1159(3)	2344(3)	59(1)
C(18)	-1515(3)	-1623(3)	1926(2)	44(1)
C(19)	184(3)	-975(3)	2244(2)	43(1)
C(20)	1303(4)	-1097(3)	3203(3)	52(1)
C(21)	2796(4)	-384(3)	3188(2)	52(1)
C(22)	2650(3)	189(3)	2209(2)	43(1)
C(23)	3927(3)	976(3)	1856(2)	42(1)
C(24)	3759(3)	1363(3)	793(2)	42(1)
C(25)	5066(4)	2251(3)	474(3)	51(1)
C(26)	4408(3)	2430(3)	-570(2)	50(1)
C(27)	2672(3)	1657(3)	-917(2)	43(1)

### Solid-state NMR

Figure 2a shows the time-domain  $^{25}\text{Mg}$  free induction decay (FID) signal for a stationary powder sample of  $\text{Mg}(\text{TPP})\text{Py}_2$ . The whole echo can be clearly seen. As explained by Massiot et al. (23), the whole-echo approach leads to a signal-to-noise enhancement by a factor of  $\sqrt{2}$ . Figure 2b shows the direct FT of the whole echo. As expected, because of the long time delay used for obtaining the whole echo signal, a large phase distortion is present in the spectrum. This distortion can be readily corrected by a linear phase correction, as shown in Fig. 2c. The  $^{25}\text{Mg}$  NMR central-transition spectrum observed for  $\text{Mg}(\text{TPP})\text{Py}_2$  exhibits an extremely large line width, ca. 260 kHz at 11.75 T. Because the width of the NMR line shape is much larger than the strength of the  $B_1$  field (50 kHz), line shape distortions are observed. To obtain accurate values of  $C_Q$  and  $\eta_Q$ , it is important to determine the precise positions of the spectral singularities in a powder pattern. To overcome the so-called "rolling off" effect from a relatively weak RF field, we obtained several spectra with the RF transmitter being set to different frequency positions. As shown in Fig. 3, the entire  $^{25}\text{Mg}$  NMR line shape depends strongly on the position of the RF transmitter. For example, when the RF transmitter

was set close to one edge of the powder line shape, the other edge shows very low intensity, as a result of low RF excitation efficiency. Using the NMR spectra shown in Figs. 3a and 3c, we obtained  $C_Q = 15.32 \pm 0.02$  MHz and  $\eta_Q = 0.00 \pm 0.05$ . These values were confirmed by analyzing an  $^{25}\text{Mg}$  QCPMG NMR spectrum obtained at 9.40 T (data not shown). It is important to point out that the above  $^{25}\text{Mg}$  quadrupole parameters were extracted from the static  $^{25}\text{Mg}$  NMR spectra by considering the second-order quadrupole interaction alone. By comparing the spectra obtained at 11.75 and 9.40 T, we have estimated that the span of the  $^{25}\text{Mg}$  chemical shielding tensor ( $\Omega = \sigma_{33} - \sigma_{11}$ ) is less than 100 ppm for  $^{25}\text{Mg}(\text{TPP})\text{Py}_2$ . This estimate is confirmed by quantum mechanical calculations, as described in the next section.

The  $^{25}\text{Mg}$  quadrupole coupling constant observed for  $\text{Mg}(\text{TPP})\text{Py}_2$  is significantly larger than all previously reported  $C_Q$  values for  $^{25}\text{Mg}$  nuclei (9). Such a large  $C_Q$  value made it very challenging to record a satisfactory solid-state  $^{25}\text{Mg}$  NMR spectrum for  $\text{Mg}(\text{TPP})\text{Py}_2$ . The observed axial symmetry for the EFG tensor is expected from the crystal structure where an approximate axial symmetry is present at the Mg site. Because of the extremely large line width of the static  $^{25}\text{Mg}$  NMR spectrum, it is not possible to obtain a reliable value for the isotropic  $^{25}\text{Mg}$  chemical shift. It is also worth noting that our attempt to record  $^{25}\text{Mg}$  NMR spectra for  $\text{Mg}(\text{TPP})\text{Py}_2$  in  $\text{CDCl}_3$  solution was unsuccessful. This may be attributed to either the rapid relaxation due to a large  $^{25}\text{Mg}$  quadrupole coupling constant or the fast ligand exchange in solution. It is also possible that both of these factors are operative. Assuming that the molecular rotational correlation for the complex is approximately 200 ps, the value of  $T_1$  and  $T_2$  was estimated to be 5.6  $\mu\text{s}$  under the extreme narrowing condition. This was much shorter than the typical probe deadtime at low frequencies. This example further illustrates the advantage of solid-state NMR over traditional solution NMR for studying low- $\gamma$  quadrupolar nuclei.

### Quantum mechanical calculations

Because we have obtained both NMR and structural information for  $\text{Mg}(\text{TPP})\text{Py}_2$ , we decided to test whether quantum mechanical calculations can reproduce the experimental NMR parameters in this Mg-porphyrin system. This attempt is of particular interest because there has been no previous theoretical work on  $^{25}\text{Mg}$  NMR parameters in organic systems. The paucity of theoretical studies on  $^{25}\text{Mg}$  NMR parameters arises primarily from the fact that very little experimental  $^{25}\text{Mg}$  NMR data are available because of the practical difficulties mentioned earlier. For comparison, we also studied a closely related Mg-porphyrin compound,  $\text{Mg}(\text{TPP})\cdot(1\text{-MeIm})_2$ .  $\text{Mg}(\text{TPP})\cdot(1\text{-MeIm})_2$  crystallizes in the tetragonal space group  $P4_2/n$  with  $Z = 4$  (21). In this compound, the Mg(II) ion is also six-coordinated to nitrogen atoms. The Mg— $N_{\text{eq}}$  bonds, 2.082 and 2.074  $\text{\AA}$ , are very similar to those found in  $\text{Mg}(\text{TPP})\text{Py}_2$ . However, the Mg— $N_{\text{ax}}$  bond length in  $\text{Mg}(\text{TPP})\cdot(1\text{-MeIm})_2$ , 2.297  $\text{\AA}$ , is much shorter than that in  $\text{Mg}(\text{TPP})\text{Py}_2$ , 2.369  $\text{\AA}$ . The calculated results for the  $^{25}\text{Mg}$  quadrupole parameters and chemical shielding tensors in  $\text{Mg}(\text{TPP})\text{Py}_2$  and  $\text{Mg}(\text{TPP})\cdot(1\text{-MeIm})_2$  are summarized in Tables 4 and 5. The data shown in Table 4 indicate that, for a given basis set, the EFG calcula-

**Table 3.** Selected bond lengths (Å) and angles (°) for Mg(TPP)-Py<sub>2</sub>.

<b>Bond lengths (Å)</b>			
Mg(1)—N(2)	2.062(2)	C(9)—C(10)	1.353(4)
Mg(1)—N(3)	2.065(2)	C(10)—C(11)	1.387(4)
Mg(1)—N(1)	2.369(2)	C(12)—C(17)	1.377(3)
N(1)—C(5)	1.321(3)	C(12)—C(13)	1.390(3)
N(1)—C(1)	1.329(3)	C(12)—C(23)	1.498(3)
C(1)—C(2)	1.369(4)	C(13)—C(14)	1.385(3)
N(2)—C(22)	1.373(3)	C(14)—C(15)	1.367(4)
N(2)—C(19)	1.377(3)	C(15)—C(16)	1.356(4)
C(2)—C(3)	1.358(4)	C(16)—C(17)	1.385(3)
N(3)—C(27)	1.371(3)	C(18)—C(19)	1.401(3)
N(3)—C(24)	1.377(3)	C(18)—C(27)#1	1.409(3)
C(3)—C(4)	1.367(4)	C(19)—C(20)	1.438(3)
C(4)—C(5)	1.362(4)	C(20)—C(21)	1.333(4)
C(6)—C(11)	1.367(3)	C(21)—C(22)	1.438(3)
C(6)—C(7)	1.372(3)	C(22)—C(23)	1.401(3)
C(6)—C(18)	1.495(3)	C(23)—C(24)	1.408(3)
C(7)—C(8)	1.377(3)	C(24)—C(25)	1.435(3)
C(8)—C(9)	1.354(4)	C(25)—C(26)	1.344(3)
		C(26)—C(27)	1.432(3)
<b>Bond angles (°)</b>			
N(2)#1-Mg(1)-N(2)	180.00(11)	C(17)-C(12)-C(13)	117.9(2)
N(2)-Mg(1)-N(3)#1	90.83(7)	C(17)-C(12)-C(23)	122.5(2)
N(2)-Mg(1)-N(3)	89.17(7)	C(13)-C(12)-C(23)	119.5(3)
N(3)#1-Mg(1)-N(3)	180.00(10)	C(14)-C(13)-C(12)	121.0(3)
N(2)-Mg(1)-N(1)#1	86.47(8)	C(15)-C(14)-C(13)	119.3(3)
N(3)-Mg(1)-N(1)#1	94.07(8)	C(16)-C(15)-C(14)	120.8(3)
N(2)-Mg(1)-N(1)	93.53(8)	C(15)-C(16)-C(17)	120.0(3)
N(3)-Mg(1)-N(1)	85.93(8)	C(12)-C(17)-C(16)	120.9(3)
N(1)#1-Mg(1)-N(1)	180.00(14)	C(19)-C(18)-C(27)#1	127.4(2)
C(5)-N(1)-C(1)	114.7(3)	C(19)-C(18)-C(6)	116.1(2)
C(5)-N(1)-Mg(1)	122.5(2)	C(27)#1-C(18)-C(6)	116.4(2)
C(1)-N(1)-Mg(1)	122.1(2)	N(2)-C(19)-C(18)	125.4(2)
N(1)-C(1)-C(2)	125.0(3)	N(2)-C(19)-C(20)	109.0(2)
C(22)-N(2)-C(19)	106.5(2)	C(18)-C(19)-C(20)	125.5(2)
C(22)-N(2)-Mg(1)	127.15(17)	C(21)-C(20)-C(19)	107.7(3)
C(19)-N(2)-Mg(1)	124.96(16)	C(20)-C(21)-C(22)	107.6(3)
C(3)-C(2)-C(1)	118.4(3)	N(2)-C(22)-C(23)	124.8(2)
C(27)-N(3)-C(24)	106.6(2)	N(2)-C(22)-C(21)	109.2(2)
C(27)-N(3)-Mg(1)	125.75(16)	C(23)-C(22)-C(21)	126.0(2)
C(24)-N(3)-Mg(1)	126.81(17)	C(22)-C(23)-C(24)	126.0(2)
C(2)-C(3)-C(4)	118.1(4)	C(22)-C(23)-C(12)	117.0(2)
C(5)-C(4)-C(3)	119.0(3)	C(24)-C(23)-C(12)	116.9(2)
N(1)-C(5)-C(4)	124.7(3)	N(3)-C(24)-C(23)	125.1(2)
C(11)-C(6)-C(7)	117.2(3)	N(3)-C(24)-C(25)	108.6(2)
C(11)-C(6)-C(18)	121.7(3)	C(23)-C(24)-C(25)	126.1(2)
C(7)-C(6)-C(18)	121.1(3)	C(26)-C(25)-C(24)	108.2(2)
C(6)-C(7)-C(8)	121.4(3)	C(25)-C(26)-C(27)	106.7(3)
C(9)-C(8)-C(7)	120.4(3)	N(3)-C(27)-C(18)#1	124.7(2)
C(10)-C(9)-C(8)	119.5(3)	N(3)-C(27)-C(26)	109.8(2)
C(9)-C(10)-C(11)	120.0(3)	C(18)#1-C(27)-C(26)	125.4(2)
C(6)-C(11)-C(10)	121.4(3)		

**Note:** Symmetry transformations used to generate equivalent atoms: #1  $-x, -y, -z$ .

tions at the Hartree–Fock (HF), B3LYP, and MP2 levels of theory show very similar results. The calculations using the 6–31G(d) basis set seems to give the best agreement between the calculated and observed <sup>25</sup>Mg quadrupole param-

eters. The  $C_Q$  values for Mg(TPP)·(1-MeIm)<sub>2</sub> are consistently smaller than those for Mg(TPP)-Py<sub>2</sub> by approximately 3–4 MHz. This is attributed to the shorter Mg—N<sub>ax</sub> bond length in Mg(TPP)·(1-MeIm)<sub>2</sub> (vide infra). Because no abso-

**Fig. 1.** Molecular structure of  $\text{Mg}(\text{TPP})\cdot\text{Py}_2$ . Hydrogen atoms are not shown for clarity.

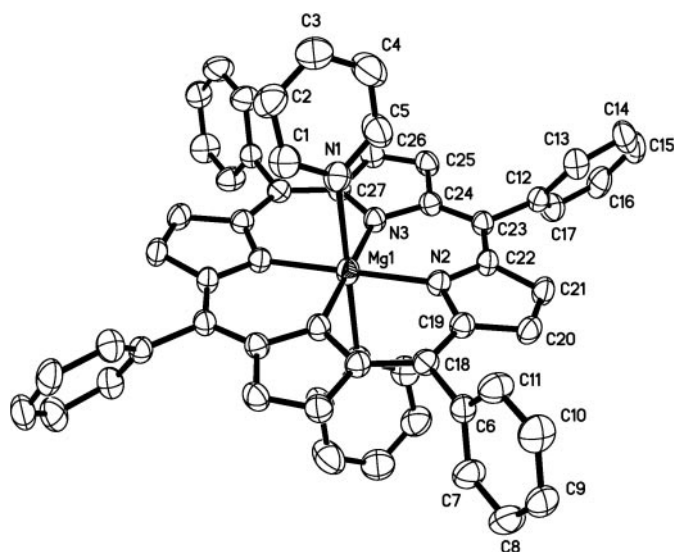
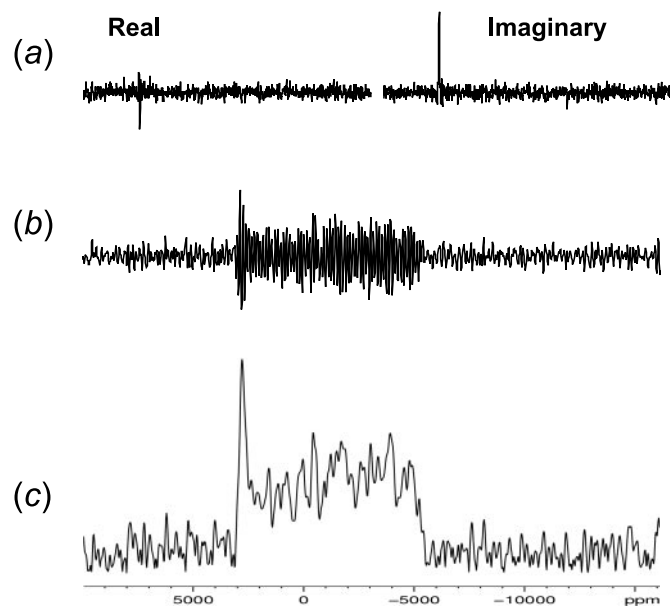
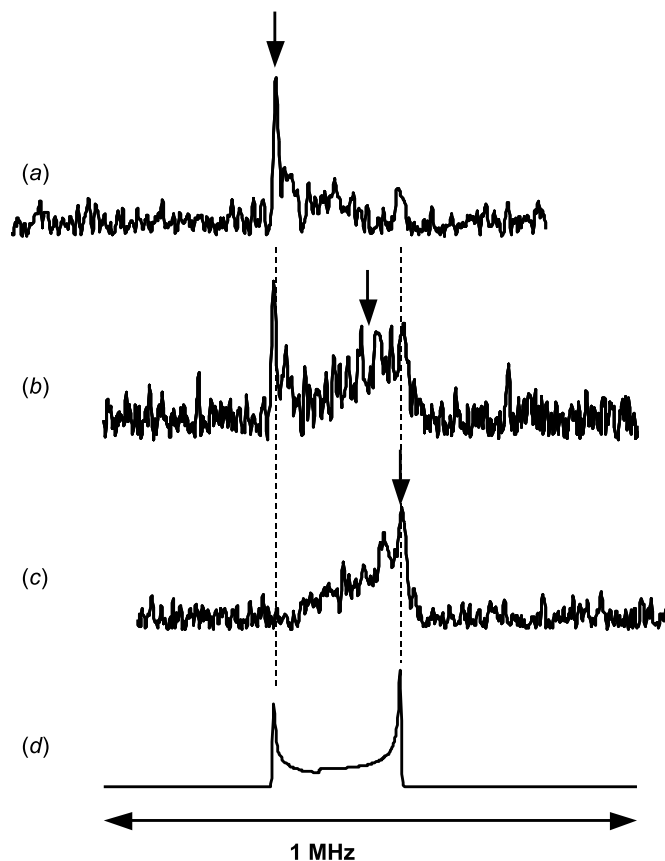


**Fig. 2.** (a) Real and imaginary parts of the  $^{25}\text{Mg}$  FID signal for  $^{25}\text{Mg}(\text{TPP})\cdot\text{Py}_2$ ; (b) Fourier transform of the whole-echo FID; (c) Phase-corrected  $^{25}\text{Mg}$  NMR spectrum. Detailed experimental parameters: transmitter offset =  $-3000$  ppm, 1 s recycle delay, 302 224 transients.



lute shielding scale for  $^{25}\text{Mg}$  is available in the literature, we decided to compute the chemical shielding constant for the referencing species,  $[\text{Mg}(\text{H}_2\text{O})_6]^{2+}$ . Using the shielding constant for  $[\text{Mg}(\text{H}_2\text{O})_6]^{2+}$ ,  $\sigma_{\text{ref}}$ , we were able to convert the calculated shielding values for  $\text{Mg}(\text{TPP})\cdot\text{Py}_2$  and  $\text{Mg}(\text{TPP})\cdot(1\text{-MeIm})_2$  into the “chemical shifts”,  $\delta_{\text{iso}} = \sigma_{\text{ref}} - \sigma_{\text{iso}}$ . The geometry of  $[\text{Mg}(\text{H}_2\text{O})_6]^{2+}$  was obtained by a full geometry optimization at the MP2/6-311G(d,p) level. The Mg—O distance is 2.105 Å and the O—H bond is 0.963 Å. The H—O—H angle for the water molecule is 105.3°. The  $[\text{Mg}(\text{H}_2\text{O})_6]^{2+}$  species has an  $O_h$  point group symmetry. To avoid the ap-

**Fig. 3.** Experimental (a, b, c) and simulated (d)  $^{25}\text{Mg}$  NMR spectra for  $^{25}\text{Mg}(\text{TPP})\cdot\text{Py}_2$ . The spectral width for each of the above spectra was 1 MHz. The arrows indicate the positions to which the RF transmitter was set. The dashed lines indicate the singularities of the powder line shape. Detailed experimental parameters are: (a) transmitter offset = 2700 ppm, 1 s recycle delay, 237 788 transients; (b) transmitter offset =  $-3000$  ppm, 1 s recycle delay, 425 216 transients; (c) transmitter offset =  $-5000$  ppm, 1 s recycle delay, 339 773 transients.



parent basis set dependence, we obtained  $\sigma_{\text{ref}}$  for each basis set. As seen from Table 5, the GIAO shielding calculations indicate that the span of the  $^{25}\text{Mg}$  chemical shielding tensor,  $\Omega = \sigma_{33} - \sigma_{11}$ , can be safely estimated to be less than 50 ppm for  $\text{Mg}(\text{TPP})\cdot\text{Py}_2$ . At 11.75 T, the line width contribution from a chemical shielding anisotropy of this magnitude would be expected to be less than 1.5 kHz in  $^{25}\text{Mg}$  NMR spectra. Since the experimental  $^{25}\text{Mg}$  NMR spectrum for  $\text{Mg}(\text{TPP})\cdot\text{Py}_2$  is 260 kHz wide at 11.75 T, it is not surprising that the  $^{25}\text{Mg}$  chemical shielding anisotropy can be ignored in our spectral analysis. For the same reason, it was also impossible to obtain experimentally a meaningful estimate for the isotropic  $^{25}\text{Mg}$  chemical shift for  $\text{Mg}(\text{TPP})\cdot\text{Py}_2$ . The GIAO shielding calculations suggest that the isotropic  $^{25}\text{Mg}$  chemical shift for an Mg(II) ion coordinated to six nitrogen ligands is approximately 10–20 ppm. We believe that this estimate is reasonably accurate; however, to our knowledge, no experimental  $^{25}\text{Mg}$  NMR data are available for six-coordinate  $\text{MgN}_6$  species.

Another piece of useful information obtained from the quantum mechanical calculations is the orientation of the

**Table 4.** Experimental and calculated  $^{25}\text{Mg}$  quadrupole parameters for  $\text{Mg}(\text{TPP})\cdot\text{Py}_2$  and  $\text{Mg}(\text{TPP})\cdot(1\text{-MeIm})_2$ .

	Method and (or) Basis set	$C_Q$ (MHz)	$\eta_Q$
$\text{Mg}(\text{TPP})\cdot\text{Py}_2$	Exptl.	$15.32 \pm 0.02$	$0.00 \pm 0.05$
	HF/6–31G(d)	15.013	0.034
	HF/6–311G(d,p)	18.524	0.047
	HF/6–311G(2d,p)	18.816	0.046
	B3LYP/6–31G(d)	14.763	0.018
	B3LYP/6–311G(d,p)	17.732	0.043
	B3LYP/6–311G(2d,p)	18.022	0.043
	MP2/6–31(d)	14.971	0.035
$\text{Mg}(\text{TPP})\cdot(1\text{-MeIm})_2$	HF/6–31G(d)	11.981	0.096
	HF/6–311G(d,p)	14.680	0.100
	HF/6–311G(2d,p)	14.969	0.103
	B3LYP/6–31G(d)	11.566	0.161
	B3LYP/6–311G(d,p)	14.164	0.103
	B3LYP/6–311G(2d,p)	14.456	0.104

**Table 5.** Calculated  $^{25}\text{Mg}$  magnetic shielding tensors for  $\text{Mg}(\text{TPP})\cdot\text{Py}_2$  and  $\text{Mg}(\text{TPP})\cdot(1\text{-MeIm})_2$ .<sup>a</sup>

	Method and (or) Basis set	$\sigma_{\text{ref}}^b$	$\delta_{\text{iso}}^c$	$\sigma_{11}$	$\sigma_{22}$	$\sigma_{33}$	$\Omega^d$
$\text{Mg}(\text{TPP})\cdot\text{Py}_2$	HF/6–31G(d)	621	11	595	603	631	36
	HF/6–311G(d,p)	609	20	572	580	616	44
	HF/6–311G(2d,p)	608	19	571	579	616	45
	B3LYP/6–31G(d)	599	9	578	589	602	24
	B3LYP/6–311G(d,p)	585	19	551	559	589	38
	B3LYP/6–311G(2d,p)	584	19	549	558	588	39
$\text{Mg}(\text{TPP})\cdot(1\text{-MeIm})_2$	HF/6–31G(d)	621	8	595	608	636	41
	HF/6–311G(d,p)	609	15	576	585	621	45
	HF/6–311G(2d,p)	608	15	574	583	621	47
	B3LYP/6–31G(d)	599	6	577	595	607	30
	B3LYP/6–311G(d,p)	585	14	555	565	594	39
	B3LYP/6–311G(2d,p)	584	14	554	563	593	39

<sup>a</sup>All magnetic shielding tensor components and isotropic chemical shifts are in ppm.

<sup>b</sup> $\sigma_{\text{ref}}$  is calculated for  $[\text{Mg}(\text{H}_2\text{O})_6]^{+2}$  with an optimized geometry at the MP2/6–311G(d,p) level.

<sup>c</sup> $\delta_{\text{iso}} = \sigma_{\text{ref}} - \sigma_{\text{iso}}$ .

<sup>d</sup>Span  $\Omega = \sigma_{33} - \sigma_{11}$ .

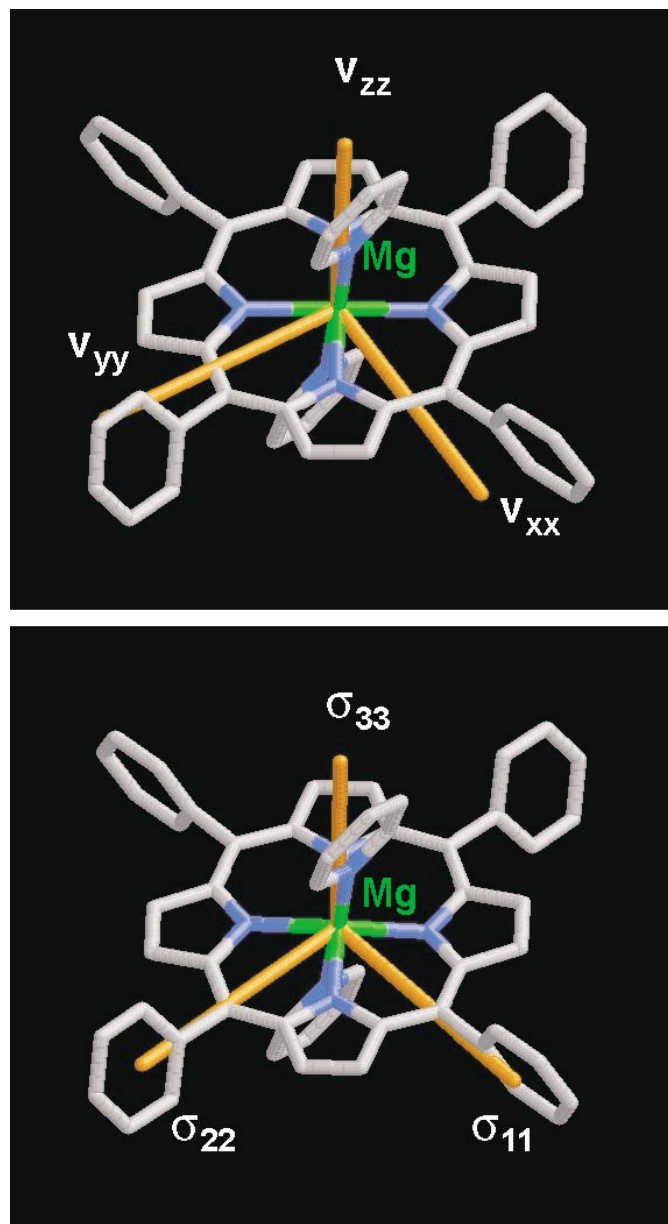
NMR tensors in the molecular frame of reference. Figure 4 shows the orientations of both EFG and chemical shielding tensors for the  $^{25}\text{Mg}$  nucleus in  $\text{Mg}(\text{TPP})\cdot\text{Py}_2$ . The largest EFG tensor component,  $V_{ZZ}$ , is  $5.3^\circ$  off the  $\text{Mg}-\text{N}_{\text{ax}}$  bond direction. The smallest EFG component,  $V_{XX}$ , lies approximately in the porphyrin plane, making an angle of  $58.6^\circ$  with respect to one of the  $\text{Mg}-\text{N}_{\text{eq}}$  bonds. The chemical shielding tensor exhibits essentially the same orientation as the EFG tensor. In particular, the tensor component with the most shielding,  $\sigma_{33}$ , is approximately  $7.5^\circ$  off the  $\text{Mg}-\text{N}_{\text{ax}}$  direction, while the tensor component with the least shielding,  $\sigma_{11}$ , lies in the porphyrin plane and makes an angle of  $45.6^\circ$  relative to the same  $\text{Mg}-\text{N}_{\text{eq}}$  bond described for the EFG tensor.

As mentioned earlier, one obvious structural feature that might be responsible for the observation of a large  $C_Q$  value at the Mg center in  $\text{Mg}(\text{TPP})\cdot\text{Py}_2$  is the large difference between  $\text{Mg}-\text{N}_{\text{eq}}$  and  $\text{Mg}-\text{N}_{\text{ax}}$  distances. To further explore the influence of the  $\text{Mg}-\text{N}_{\text{ax}}$  bond on the EFG at the Mg center, we performed a series of EFG calculations for a model where the position of the axial pyridine ligands is systematically varied. The geometry of the porphyrin core in

the model is identical to that in  $\text{Mg}(\text{TPP})\cdot\text{Py}_2$ . The results are shown in Table 6 and depicted in Fig. 5. It is interesting to see that the value of  $C_Q$  increases monotonically with the increase of  $\text{Mg}-\text{N}_{\text{ax}}$  bond distance. As shown in Table 6, the calculation also gave an estimate for an Mg(II) ion in a square-planar binding geometry,  $C_Q \approx 22$  MHz. At 11.75 T, this  $C_Q$  value would correspond to a central-transition  $^{25}\text{Mg}$  NMR spectrum two times wider than the one shown in Fig. 2c. On the basis of these results, we believe that many Mg–porphyrin complexes should be accessible by solid-state  $^{25}\text{Mg}$  NMR at currently available high magnetic fields (from 11.75 to 21.15 T).

It is also of interest to compare the EFG tensor observed for  $\text{Mg}(\text{TPP})\cdot\text{Py}_2$  with those reported for two isostructural TPP complexes,  $\text{Fe}^{\text{II}}(\text{TPP})\cdot\text{Py}_2$  and  $\text{Co}^{\text{III}}(\text{TPP})\cdot\text{Py}_2$ . From a Mössbauer experiment, Kobayashi et al. (24) reported an  $^{57}\text{Fe}$  quadrupole splitting for  $\text{Fe}^{\text{II}}(\text{TPP})\cdot\text{Py}_2$  (low spin) at 300 K,  $\Delta E_Q = 1.22$  mm  $\text{s}^{-1}$ . This quadrupole splitting corresponds to  $V_{ZZ} = 0.75$  au, assuming  $Q(^{57}\text{Fe}) = 16.0 \times 10^{-30}$  m<sup>2</sup>. This EFG value is much larger than the corresponding value found at the Mg nucleus in  $\text{Mg}(\text{TPP})\cdot\text{Py}_2$ ,  $V_{ZZ} = 0.3202$  au. As illustrated in Fig. 5, the  $V_{ZZ}$  value is a function of the

**Fig. 4.** Orientations of the  $^{25}\text{Mg}$  EFG tensor (top) and the chemical shielding tensor (bottom) in the molecular frame of  $\text{Mg}(\text{TPP})\cdot\text{Py}_2$ . Quantum mechanical calculations were done at the HF/6-31G(d) level.



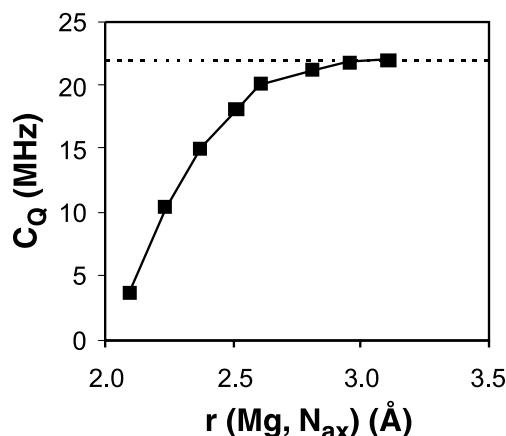
$\text{M}-\text{N}_{\text{ax}}$  distance. In  $\text{Fe}^{\text{II}}(\text{TPP})\cdot\text{Py}_2$ , however, the  $\text{Fe}-\text{N}_{\text{ax}}$  bond length, 2.039 Å, is similar to the  $\text{Fe}-\text{N}_{\text{eq}}$  bonds, 1.989 and 1.997 Å (25). This immediately suggests that the  $d^6$  metal TPP complexes behave differently as the  $\text{Mg}-\text{TPP}$  compounds. In  $\text{Co}^{\text{III}}(\text{TPP})\cdot\text{Py}_2$ , the  $V_{\text{ZZ}}$  value at the metal center is 0.167 au, as reported by Medek et al. from a solid-state  $^{59}\text{Co}$  NMR study (5g). This value is much smaller than that in  $\text{Fe}^{\text{II}}(\text{TPP})\cdot\text{Py}_2$ . This may be explained by a general trend, in which the  $\text{M}-\text{N}_{\text{ax}}$  distance is usually smaller in  $\text{Co}^{\text{III}}-\text{TPP}$  complexes than in  $\text{Fe}^{\text{II}}-\text{TPP}$  complexes (21). In this regard, the  $d^6$  metal-TPP compounds exhibit a similar  $\text{M}-\text{N}_{\text{ax}}$  dependence to that observed for  $\text{Mg}-\text{TPP}$  complexes.

**Table 6.** Calculated dependence of the  $^{25}\text{Mg}$  quadrupole parameters on the  $\text{Mg}-\text{N}_{\text{ax}}$  distance in  $\text{Mg}(\text{TPP})\cdot\text{Py}_2$  at the HF/6-31G(d) level.

$R(\text{Mg}-\text{N}_{\text{ax}})$ (Å)	$C_Q$ (MHz)	$\eta_Q$
2.091	3.677	0.070
2.233	10.502	0.042
2.369	15.013	0.034
2.510	18.056	0.032
2.604	20.094	0.032
2.807	21.151	0.033
2.952	21.716	0.034
3.103	21.987	0.036
$+\infty^a$	21.988	0.038

<sup>a</sup>Calculated without axial ligands.

**Fig. 5.** Calculated dependence of  $C_Q(^{25}\text{Mg})$  on the  $\text{Mg}-\text{N}_{\text{ax}}$  bond length in  $\text{Mg}(\text{TPP})\cdot\text{Py}_2$ . The dashed line indicates the  $C_Q(^{25}\text{Mg})$  value for an  $\text{Mg}-(\text{TPP})$  complex without axial ligands.



## Conclusion

We have reported solid-state  $^{25}\text{Mg}$  NMR, crystallographic, and computational results for an  $\text{Mg}(\text{II})$ -porphyrin complex,  $\text{Mg}(\text{TPP})\cdot\text{Py}_2$ . The  $^{25}\text{Mg}$  quadrupole coupling constant observed for  $\text{Mg}(\text{TPP})\cdot\text{Py}_2$ ,  $C_Q = 15.32 \pm 0.02$  MHz, is the largest so far reported for  $^{25}\text{Mg}$  nuclei. The  $^{25}\text{Mg}$  chemical shielding anisotropy is, however, too small to be measured reliably. We have performed quantum mechanical calculations for the  $^{25}\text{Mg}$  NMR tensors in two related  $\text{Mg}$ -porphyrin complexes:  $\text{Mg}(\text{TPP})\cdot\text{Py}_2$  and  $\text{Mg}(\text{TPP})\cdot(1-\text{MeIm})_2$ . Quantum mechanical calculations were carried out at various levels of theory including restricted Hartree-Fock, density functional theory, and MP2 with different basis sets. The calculations with a 6-31G(d) basis set have reproduced reasonably well the observed  $^{25}\text{Mg}$  NMR data for  $\text{Mg}(\text{TPP})\cdot\text{Py}_2$ . The calculations also suggest that the span of the  $^{25}\text{Mg}$  chemical shift tensor is less than 50 ppm for  $\text{Mg}(\text{TPP})\cdot\text{Py}_2$ .

To obtain an upper limit for the  $^{25}\text{Mg}$  quadrupole coupling constant in  $\text{Mg}$ -porphyrin systems, we have performed quantum mechanical calculations for an  $\text{Mg}(\text{II})$  ion at the center of a porphyrin moiety without axial ligands, which represents the most asymmetrical environment for the  $\text{Mg}$  cation. For such a model, the  $^{25}\text{Mg}$  quadrupole coupling

constant is approximately 22 MHz. This may suggest that most of Mg(II)–porphyrin complexes should be accessible by high-field  $^{25}\text{Mg}$  NMR. The present work represents the first solid-state  $^{25}\text{Mg}$  NMR study for an Mg(II)–porphyrin system. Extension of this research to chlorophyll models is under way in this laboratory.

## Acknowledgment

This work was supported by equipment and research grants from the Natural Sciences and Engineering Research Council (NSERC) of Canada (to G.W. and S.W.). G.W. thanks Queen's University for a Chancellor's Research Award (2000–2004) and the Province of Ontario for a Premier's Research Excellence Award (2000–2004). A.W. thanks Queen's University for an R.S. McLaughlin Fellowship (2000–2002) and the Province of Ontario for an Ontario Graduate Scholarship (OGS) (2002–2003). We are also grateful to Ramsey Ida for assistance in quantum mechanical calculations and to Professor Robert W. Schurko (University of Windsor) for obtaining an  $^{25}\text{Mg}$  QCPMG spectrum at 9.40 T. All quantum mechanical calculations were performed at the High Performance Computing Virtual Laboratory (HPCVL) at Queen's University.

## References

1. K.M. Kadish, K.M. Smith, and R. Guilard (*Editors*). The porphyrin handbook. Academic Press, Burlington, MA. 1999.
2. L.R. Milgrom. The colours of life: An introduction to the chemistry of porphyrins and related compounds. Oxford University Press, New York. 1997.
3. J.E. Falk. Porphyrins and metalloporphyrins. Elsevier, Amsterdam. 1975.
4. F.A. Walker. *Coord. Chem. Rev.* **185/186**, 471 (1999); and refs. therein.
5. (a) H.J. Jakobsen, P.D. Ellis, R.R. Inners, and C.F. Jensen. *J. Am. Chem. Soc.* **104**, 7442 (1982); (b) G.N. La Mar, C.M. Dellinger, and S.S. Sankar. *Biochem. Biophys. Res. Commun.* **128**, 628 (1985); (c) H.C. Lee, J.K. Gard, T.L. Brown, and E. Oldfield. *J. Am. Chem. Soc.* **107**, 4087 (1985); (d) L. Baltzer. *J. Am. Chem. Soc.* **109**, 3479 (1987); (e) M.A. Kennedy and P.D. Ellis. *J. Am. Chem. Soc.* **111**, 3195 (1989); (f) J. Chung, H.C. Lee, and E. Oldfield. *J. Magn. Reson.* **90**, 148 (1990); (g) A. Medek, V. Frydman, and L. Frydman. *J. Chem. Phys. B*, **101**, 8959 (1997).
6. (a) M.T. McMahon, A.C. deDios, N. Godbout, R. Salzmann, D.D. Laws, H. Le, R.H. Havlin, and E. Oldfield. *J. Am. Chem. Soc.* **120**, 4784 (1998); (b) N. Godbout, L.K. Sanders, R. Salzmann, R.H. Havlin, M. Wojdelski, and E. Oldfield. *J. Am. Chem. Soc.* **121**, 3829 (1999).
7. H. Scheer (*Editor*). Chlorophylls. CRC Press, Boca Raton, Florida. 1991.
8. (a) R.G. Bryant. *J. Magn. Reson.* **6**, 159 (1972); (b) S. Forsén, T. Andersson, T. Drakenberg, O. Teleman, and H.J. Vogel. *In Calcium binding proteins*. Edited by B. de Bernad. Elsevier, Amsterdam. 1983; (c) T. Shimizu and M. Hatano. *Inorg. Chem.* **24**, 2003 (1985); (d) M.-D. Tsai, T. Drakenberg, E. Thulin, and S. Forsén. *Biochemistry* **26**, 3635 (1987); (e) S.S. Reid and J.A. Cowan. *Biochemistry* **29**, 6025 (1990); (f) S.S. Reid and J.A. Cowan. *J. Am. Chem. Soc.* **113**, 673 (1991); (g) J.A. Cowan. *Inorg. Chem.* **30**, 2740 (1991); (h) J.A. Cowan. *J. Am. Chem. Soc.* **113**, 675 (1991); (i) E. Berggren, L. Nordenskiöld, and W.H. Braunlin. *Biopolymers*, **32**, 1339 (1992); (j) L. Wright and L.E. Lerner. *Biopolymers*, **34**, 691 (1994).
9. (a) M.E. Smith. *Ann. Rep. NMR Spectrosc.* **43**, 121 (2001) and refs. therein; (b) F.H. Larsen, J. Skibsted, H.J. Jakobsen, and N.C. Nielsen. *J. Am. Chem. Soc.* **122**, 7080 (2000).
10. S. Sham and G. Wu. *Inorg. Chem.* **39**, 4 (2000).
11. C.V. Grant, V. Frydman, and L. Frydman. *J. Am. Chem. Soc.* **122**, 11 743 (2000).
12. J.S. Lindsey and J.N. Woodford. *Inorg. Chem.* **34**, 1063 (1995).
13. S.J. Baum, B.F. Burnham, and R.A. Plane. *Proc. Natl. Acad. Sci. U.S.A.* **52**, 1439 (1964).
14. A.C. Kunwar, G.L. Turner, and E. Oldfield. *J. Magn. Reson.* **69**, 124 (1986).
15. R. Dupree and M.E. Smith. *Chem. Commun.* 1483 (1988).
16. Bruker AXS. 1995. SHELXTL Crystal structure analysis package [computer program]. Version 5. Bruker AXS, Analytical X-ray System, Siemens, Madison, WI.
17. D.T. Cromer and J.T. Waber. *International tables for X-ray crystallography*. Kynoch Press, Birmingham, U.K. 1974.
18. M.J. Frisch, G.W. Trucks, H.B. Schlegel, G.E. Scuseria, M.A. Robb, J.R. Cheeseman, V.G. Zakrzewski, J.A. Montgomery, R.E. Stratmann, J.C. Burant, S. Dapprich, J.M. Millam, A.D. Daniels, K.N. Kudin, M.C. Strain, O. Farkas, J. Tomasi, V. Barone, M. Cossi, R. Cammi, B. Mennucci, C. Pomelli, C. Adamo, S. Clifford, J. Ochterski, G.A. Petersson, P.Y. Ayala, Q. Cui, K. Morokuma, D.K. Malick, A.D. Rabuck, K. Raghavachari, J.B. Foresman, J. Cioslowski, J.V. Ortiz, B.B. Stefanov, G. Liu, A. Liashenko, P. Piskorz, I. Komaromi, R. Gomperts, R.L. Martin, D.J. Fox, T. Keith, M.A. Al-Laham, C.Y. Peng, A. Nanayakkara, C. Gonzalez, M. Challacombe, P.M.W. Gill, B. Johnson, W. Chen, M.W. Wong, J.L. Andres, M. Head-Gordon, E.S. Replogle, and J.A. Pople. 1998. Gaussian98 [computer program]. Revision A.6. Gaussian, Inc., Pittsburgh, PA.
19. P. Pyykkö. *Mol. Phys.* **99**, 1617 (2001).
20. (a) R. Ditchfield. *Mol. Phys.* **27**, 789 (1974); (b) K. Wolinski, J.F. Hilton, and P. Pulay. *J. Am. Chem. Soc.* **112**, 8257 (1990).
21. V. McKee, C.C. Ong, and G.A. Rodley. *Inorg. Chem.* **23**, 4242 (1984).
22. R. Bonnett, M.B. Hursthouse, K.M.A. Malik, and B. Mateen. *J. Chem. Soc., Perkin Trans. 2*, 2072 (1977).
23. D. Massiot, I. Farnan, N. Gautier, D. Trumeau, A. Trokiner, and J.P. Coutures. *Solid State Nucl. Magn. Reson.* **4**, 241 (1995).
24. H. Kobayashi, Y. Maeda, and Y. Yanagawa. *Bull. Chem. Soc. Jpn.* **43**, 2342 (1970).
25. N. Li, V. Petricek, P. Coppens, and J. Landrum. *Acta Crystallogr. Sect. C*, **41**, 902 (1985).